arXiv:1604.02775v1 [cond-mat.mtrl-sci] 11 Apr 2016

Strain enhanced superconductivity of MoX_2 (X=S or Se) bilayers with Na intercalation

Jun-Jie Zhang, Bin Gao, and Shuai Dong*
Department of Physics, Southeast University, Nanjing 211189, China
(Dated: April 12, 2016)

MoX_2 (X=S or Se) is a semiconductor family with two-dimensional structure. And a recent calculation predicted the superconductivity in electron doped MoS_2 monolayer. In this work, the electronic structure and lattice dynamics of MoX_2 bilayers with monolayer Na intercalated, have been calculated. According to the electron-phonon interaction, it is predicted that these bilayers can be transformed from indirect-gap semiconductors to a superconductors by Na intercalation. More interestingly, the biaxial tensile strain can significantly enhance the superconducting temperature up to ~ 10 K in Na-intercalated MoS_2. In addition, the phonon mean free path at room-temperature is also greatly improved in Na intercalated $MoSe_2$, which is advantaged for related applications.

PACS numbers: 63.22.Np, 74.78.-w, 65.80.-g

I. INTRODUCTION

Two-dimensional (2D) material such as graphene, black phosphorus, and layered transition metal dichalcogenides (TMDs) have attracted enormous interest for their unique structure, novel physical properties, and broad potential applications. Superior to the semimetallic graphene, few-layer MoS_2's show moderate band gaps which are crucial for practical on/off ratio in electronic circuit devices.[1] Besides, MoS_2 is potentially important in optoelectronic because its band gap is in the visible light range.[2] For this reason, great efforts have been made to investigate the dynamics of various carriers in MoS_2 including mobilities of electrons, excitons, as well as phonons.[3–6]

Structurally, each layer of MoS_2 (as well as $MoSe_2$) is constructed by the S-Mo-S (or Se-Mo-Se) sandwich, as shown in Fig. 1. Along the c-axis, the neighboring triatomic layer is weakly coupled by van der Waals (vdw) interaction.[7] This layered nature makes MoS_2 (or $MoSe_2$) flexible and tailorable, e.g. to be doped by ion absorption or intercalation, as well as to fabricate heterostructures.[8–10] These artificial modificatory MoS_2 and $MoSe_2$ show lots of extraordinary qualities. For example, a giant Rashba-type splitting was found in MoS_2/Bi(111) heterostructure,[8] and a half-metal behavior was predicted in Fe adatoms adsorbed on monolayer and bilayer MoS_2 sheets.[9] Recently, the electron-doped monolayer MoS_2 was predicted to be a BCS-type superconductor with a considerable critical temperature (T_C) up to 20 K when one extra electron artificially-added per chemical unit.[10] However, by considering realistic doping methods (e.g. K absorption),[10] the calculated T_C was far below the expected value. Experimentally, an early work by Woollam *et. al.* studied the insertion of K/Na atoms into bulk MoS_2, which found the maximum superconducting T_C's of K_xMoS_2 and Na_xMoS_2 to be about 7 K and 3.2 K respectively.[11] In this sense, the electron doped MoS_2 should be a promising superconductor although its real T_C is seriously suppressed by real doping methods. Very recently, the dynamical stability and superconductivity have been reported in the free-standing Li-intercalated MoS_2.[12] However, in real situation these 2D few layers are putted on particular substrates and will be affected by the lattice mismatch, which have not been addressed in Ref. 12.

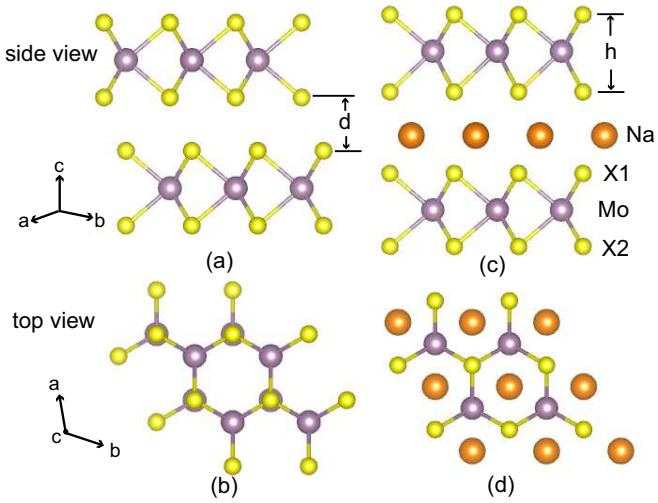

FIG. 1. (Color online) Side and top views of atomic structures of MoX_2 bilayer [(a) and (b)] and (MoX_2)$_2$Na system [(c) and (d)].

In this work, the lattice dynamics and electron-phonon (EP) coupling of Na-intercalated MoS_2 and $MoSe_2$ bilayers have been studied via first-principles density functional theory (DFT) and density function perturbation theory (DFPT). Our calculations confirm the superconductivity in MoS_2 and $MoSe_2$ with Na intercalation. More interestingly, this superconductivity can be significantly enhanced by tensile strain. Our calculations will motivate more experimental studies to tune the physical properties like superconductivity of 2D materials by the strain effect.

II. MODEL & METHODS

The DFT calculations have been performed using the PWSCF program of the Quantum-ESPRESSO distribution.[13] The ultrasoft pseudo-potential (including the semicore electrons as valence electrons in case of Mo) and generalized gradient approximation of Perdew-Burke-Ernzerhof (GGA-PBE) are used with a cutoff energy 35 Ry for the expansion of the electronic wave function in the plane waves. The vdw interactions are treated using the (Grimme) DFT-D2 approximation.[14]

MoX_2 bilayers are modeled using slabs with one Na layer (one Na per one unit cell area) inserted. The surfaces are simulated by adding a vacuum layer of $\sim$ 15 Å. For the electronic structure calculations, the Brillouin zone (BZ) integrations are performed with an $18\times18\times1$ grid by using the first-order Hermite-Gaussian smearing technique. Within the framework of the linear response theory, the dynamical matrices are calculated for $6\times6\times1$ grid of special q points in the irreducible two-dimensional BZ and are Fourier interpolated throughout the full Brillouin zone. The dense $36\times36\times1$ grid is used in the BZ integrations in order to produce the accurate electron-phonon (EP) interaction matrices.

III. RESULTS & DISCUSSION

A. Crystalline & electronic structures

Although the stablest MoX_2 bilayers are stacked as the A-B type (Fig. 1(a-b)),[15] this type of stacking conformation becomes dynamic unstable when Na monolayer is interacted into the MoX_2 bilayers, as evidenced by the imaginary frequencies of phonon spectrum around Γ point. Alternatively, the A-A type stacking conformation (Fig. 1(c-d)) is dynamic stable, which will be further discussed in Sec.III.B. Similar conclusion was also recently reported in Li-interacted MoS_2 bilayer.[12] Therefore, considering the dynamic stabilization, the conformation as sketched in Fig. 1(d) will be systematically studied in the following. Each primitive cell contain two MoX_2 layers and one Na atom.

First, the relaxation is performed until the force on each atom is smaller than 10^{-4} Ry/a.u.. The optimized lattice constant and interatomic distances are listed in Table I in comparison with the experimental values. The calculated lattice constant is only slight larger than the experimental value, which is quite reasonable since GGA normally overestimates lattice constants.

The calculated electron density difference are visualized in Fig. 2, which indicates the spatial distribution difference of electron density between the pure MoX_2 bilayer and Na-intercalated MoX_2 bilayer. The charge transfer from Na to $X1$ is obvious, especially for X=S, which changes the vdw force between original bilayers to ionic-bond-like interactions between Na and $X1$. As a direct result, the layer distance (d) is significantly shorten,

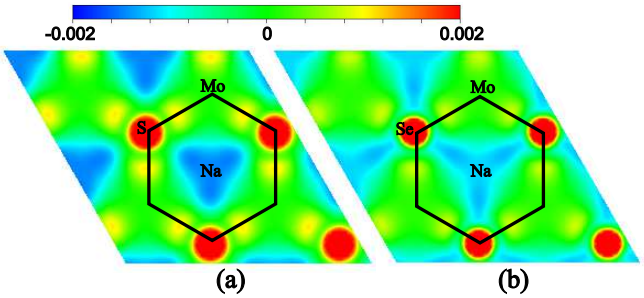

FIG. 2. (Color online) Electron density difference viewed along the (001) direction for (a) $(MoS_2)_2$Na and (b) $(MoSe_2)_2$Na.

TABLE I. The optimized structural parameters (as defined in Fig. 1) in unit of Å. The experimental values (with the superscript E) are also listed.[16,17]

	MoS_2^E	MoS_2	$(MoS_2)_2$Na	$MoSe_2^E$	$MoSe_2$	$(MoSe_2)_2$Na
a	3.161	3.204	3.251	3.285	3.330	3.385
h	3.072	3.119	3.130	3.225	3.344	3.346
d	3.074	3.113	2.249	3.225	3.178	2.435

as listed in Table I.

The calculated band structures and density of states (DOS) are shown in Fig. 3. As expected, the Fermi level crosses the conduction band as a direct result of Na intercalation, which dopes electrons to $X1$'s p orbitals and builds strong ionic bonding between Na-X. It should be noted that this intercalation is different from previously studied Na-adsorption on MoS_2 by Komesu *et.al.*,[18] who found a semiconductor behavior with a narrowed band gap.

B. Phonon, electron-phonon coupling, & superconductivity

Then we turn to pay attention to the phonon modes at the zone center. The pure MoS_2 and $MoSe_2$ bilayers have the identical point group (D_{3d}), which is reduced to D_{3h} in $(MoX_2)_2$Na. For the D_{3d} point group, the optical modes at BZ center Γ point can be decomposed as $3A_{1g}\oplus2A_{2u}$ polarized along the hexagonal c axis direction and $3E_g\oplus2E_u$ polarized in the hexagonal closed packed plane. The phonon modes E_g and A_{1g} are both Raman (R) active, while the A_{2u} and E_u modes are infrared (IR) active, as sketched in Fig. 4(a). In contrast, for the D_{3h} point group, the optical modes at Γ point can be decomposed as $A_2''\oplus A_1'\oplus E'\oplus E''$. A_2'' and E'' are infrared active, while A_1' and E' are Raman active. The calculated frequencies of these optical modes are listed in Table II, in comparison with some experimental data.

For pure MoX_2 bilayers, the calculated phonon frequencies are only slightly smaller than the corresponding experimental values.[19] This tiny inaccuracy is un-

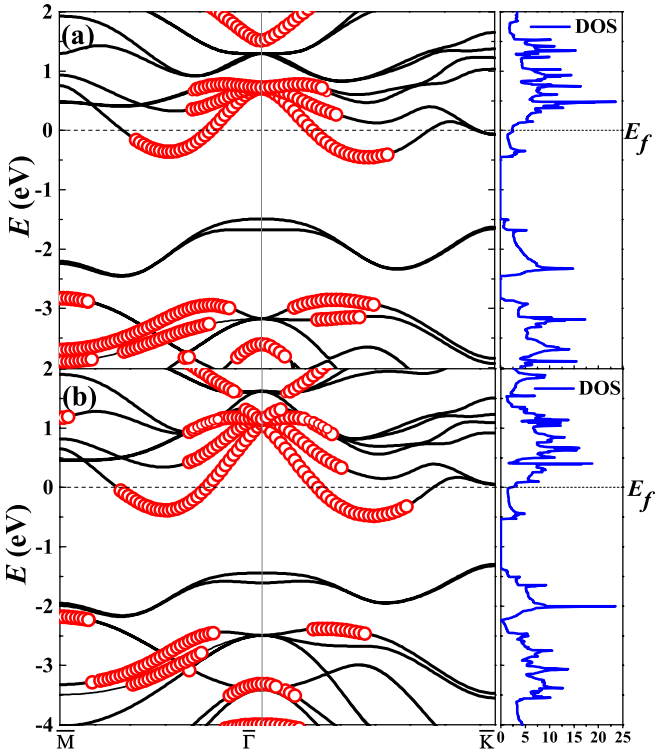

FIG. 3. (Color online) Electronic band structures and DOS's. The red circles indicate those states with more than 50% of density contributed by Na and $X1$. (a) $(MoS_2)_2Na$; (b) $(MoSe_2)_2Na_2$.

TABLE II. The calculated frequencies (in unit of cm^{-1}) of vibratory modes at Γ point for $(MoX_2)_2Na$ system and pure MoX_2 bilayer. The experimental values of A^2_{1g} (A^2_{2u}) and E^1_g (E^1_u) for pure MoS_2 ($MoSe_2$) bilayer are 406.1 cm^{-1} (242.8 cm^{-1}) and 384.9 cm^{-1} (287.1 cm^{-1}), respectively.[19]

R	A^1_{1g}	A^2_{1g}	E^1_g	E^2_g	A^3_{1g}	E^3_g
MoS_2	464.3	398.9	376.7	280.9	25.6	20.3
$MoSe_2$	345.1	237.6	277.6	163.7	36.2	18.7
R	$A'_1(1)$	$A'_1(2)$	$E'(1)$	$E'(2)$	$A'_1(3)$	$E'(3)$
$(MoS_2)_2Na$	416.9	329.0	349.3	260.6	39.0	15.9
$(MoSe_2)_2Na$	313.2	206.3	260.4	154.8	29.5	19.2
IR	A^1_{2u}	A^2_{2u}	E^1_u	E^2_u		
MoS_2	462.6	405.4	376.7	280.2		
$MoSe_2$	344.1	235.7	277.1	163.1		
IR	$A''_2(1)$	$A''_2(2)$	$E''(1)$	$E''(2)$		
$(MoS_2)_2Na$	416.5	321.3	349.3	257.1		
$(MoSe_2)_2Na$	311.7	205.2	260.6	156.0		

derstandable since the GGA-PBE pseudo-potential normally overestimates the volume of cell, which softens the phonon modes. For $(MoX_2)_2Na$ systems, there are considerable red shifts of phonon frequencies compared to the corresponding ones of pure MoX_2 bilayers except $A'_1(3)$ for $(MoS_2)_2Na$ and $E'(3)$ for $(MoSe_2)_2Na$. On one hand, the expanded lattice structure by the intercalated Na layer (e.g. see a's and h's in Table I) leads to weaker force constants between X-Mo, which softens phonon modes. In fact, due to a larger lattice constant of $(MoSe_2)_2Na$ compared with $(MoS_2)_2Na$, the frequencies of phonon modes in $(MoSe_2)_2Na$ are correspondingly smaller than those of $(MoS_2)_2Na$. On the other hand, the aforementioned charge transfer from Na to $X1$ makes the $X1$-Na links be strongly ionic-type, which may suppress the neighbor covalent X-Mo bonds as a side effect. The $A'(3)$ and $E'(3)$ mode, which are layer and shear breathing modes respectively, are sensitive to the interlayer interaction. Due to the electronegativity difference between S and Se, more (less) charge is transferred from Na to neighboring S (Se), making stronger (weaker) Coulomb attraction between Na monolayer and MoS_2 ($MoSe_2$) layers. Thus, the changes of $A'(3)$ and $E'(3)$ modes in $Na(MoSe_2)_2$ are analogous to the trilaminar $MoSe_2$ case,[19] i.e. $A'(3)$ is softening and $E'(3)$ is stiffening. In contrast, the strong Coulomb attraction between Na monolayer and MoS_2 layer moves these two modes toward opposite directions, i.e. $A'(3)$ is blue shifted and $E'(3)$ is red shifted, similar to the Li-intercalated MoS_2 case.[12]

The calculated phonon dispersions along major high symmetry lines and phonon densities of states (PDOS, $F(\omega)$) for $(MoX_2)_2Na$ are shown in Fig. 4(b-e). No imaginary frequency exists in the full phonon spectra, indicating the dynamical stability of the calculated structures of $(MoX_2)_2Na$. Since Na's vibration modes own the identical symmetry to these X-Mo-X ones, the phonon eigenvectors have a strongly mixed character of Na atom and MoX_2 triatomic layer, as indicated in Fig. 4(b-c). It is clear that the vibrations contributed by Na are in the intermediate- and low-frequency region, as well as the out-of-plane acoustic mode (ZA). Generally, the acoustic modes and the layer-breathing modes for opposite vibrations of two triatomic layers are in the low-frequency range and the sandwich X-Mo-X bond-stretching modes are in the high-frequency range due to the strong covalent bonding.[20] As shown in Fig. 4(b), two interlayer-shear modes [E'(TO): optical in-plane transverse mode, E'(LO): optical in-plane longitudinal mode] and one interlayer-breathing mode [A''_2(ZO): optical out-plane mode] are highly mixed with the Na layer's contribution, especially for the E'(LO) mode. And due to the moderate Coulomb attraction between Na and neighboring $X1$ ions, these E'(TO), E'(LO), and A''_2(ZO) modes situate in the intermediate frequency region.

In the following, the EP interaction is estimated. According to the Migdal-Eliashberg theory, the Eliashberg spectral function $[\alpha^2F(\omega)]$ is given by:[21]

$$\alpha^2F(\omega) = \frac{1}{N(E_f)}\sum_{\nu}\sum_{kqjj'}\left|g^{q\nu}_{(k+q)j'kj}\right|^2 \delta(\varepsilon_{kj}-\varepsilon_F)\delta(\varepsilon_{(k+q)j}-\varepsilon_F)\delta(\omega-\omega_{q\mu}) \quad (1)$$

where $N(E_f)$ is the electronic DOS at Fermi level;

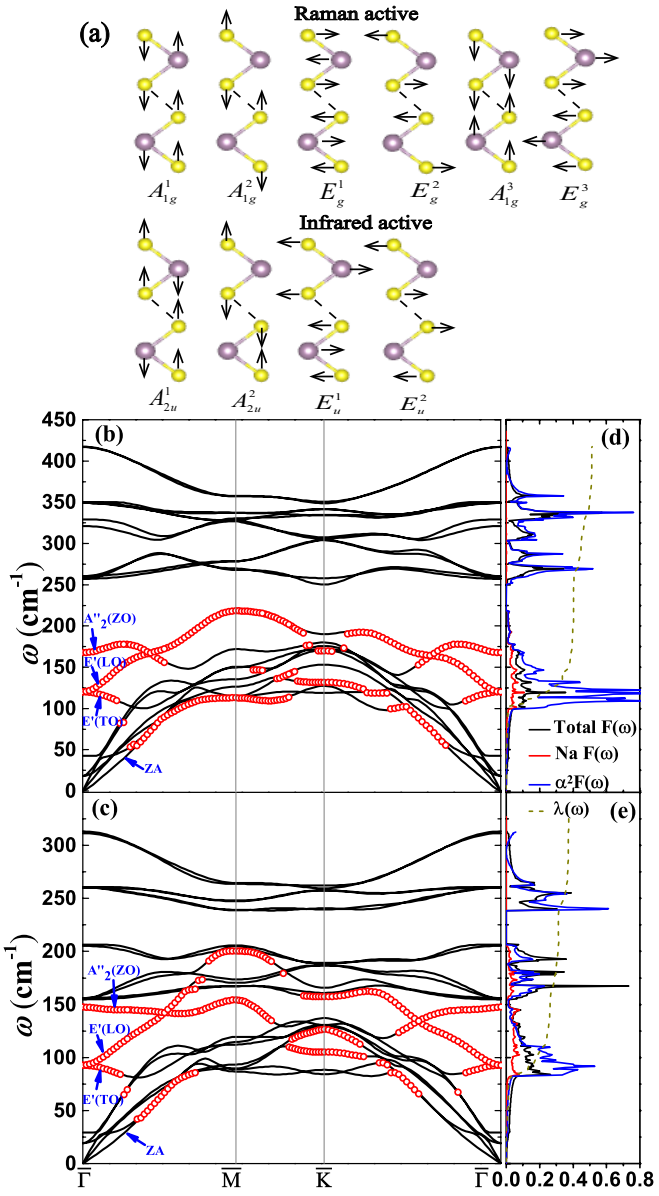

FIG. 4. (Color online) (a) Sketch of vibration modes of MoX_2 bilayer. (b-c) Calculated phonon dispersion, phonon DOS, electron-phonon coupling λ, and Eliashberg spectral function for $(MoS_2)_2Na$ system [(b) and (d)] and for $(MoSe_2)_2Na$ system [(c) and(e)].

$g^{q\nu}_{(k+q)j'kj}$ is the EP matrix element which can be determined self-consistently by the linear response theory. The EP coupling coefficient λ is obtained by evaluating:[22]

$$\lambda = 2\int_0^\infty \frac{\alpha^2F(\omega)}{\omega}d\omega. \quad (2)$$

The calculated coefficents are summarized in Table III and the Eliashberg functions for $(MoX_2)_2Na$ are shown in Fig. 4(c-d). The similarity between $F(\omega)$ and $\alpha^2F(\omega)$ indicates that all vibration modes contribute to the EP interaction. However, those high-frequency phonons do not contribute much to the strength of electron-phonon interaction due to the weighting of $1/\omega$ in the definition of λ (see Eq. 2).

TABLE III. Calculated superconducting T_C in unit of K, electron-phonon coupling λ, logarithmically averaged frequency ω_{ln} (in unit of K) and electronic DOS at Fermi level $N(E_f)$ (states/eV).

	$N(E_f)$	ω_{ln}	λ	T_C
$(MoS_2)_2Na$	2.377	219.452	0.509	2.858
$(MoSe_2)_2Na$	2.143	177.137	0.373	0.484

According to Fig. 4(d-e), it's obvious that E'(TO), E'(LO), and A_2''(ZO) modes in $(MoX_2)_2Na$ make great contribution to λ by increasing $\alpha^2F(\omega)$ curve peak in the low frequency region. As summarized in Table III, λ is larger in $(MoS_2)_2Na$ than in $(MoSe_2)_2Na$. The physical reasons are: 1) Larger DOS value at the Fermi level in $(MoS_2)_2Na$; 2) The contribution from E'(TO), E'(LO), and A_2''(ZO) modes are stronger in $(MoS_2)_2Na$.

The superconducting T_C can be estimated using the Allen-Dynes modified McMillan equation:[23]

$$T_C = \frac{\omega_{ln}}{1.2}\exp[-\frac{1.04(1+\lambda)}{\lambda-\mu^*(1+0.62\lambda)}], \quad (3)$$

where μ^* is the Coulomb repulsion parameter and ω_{ln} is the logarithmically averaged frequency. When taking a typical value $\mu^* = 0.1$, the calculated T_C is 2.858 K for $(MoS_2)_2Na$, which is very close to the measured values (about 2.2-3.2 K) for Na-doped MoS_2 bulk.[11] However, the obtained T_C (0.484 K) for $(MoS_2)_2Na$ is very low.

The substrate strain from lattice mismatch is a widely used method to tune the physical properties of 2D materials, e.g. zero-field quantum Hall effect in graphene.[24] Then it is interesting to study the lattice mismatch effect to the superconducting T_C of Na-intercalated MoX_2.

The biaxial strain (ϵ) is imposed to simulate the lattice mismatch and the results are shown in Fig. 5. Interestingly, for $(MoS_2)_2Na$ with increasing tensile strain, T_C continuously increases to a maximum value 10.049 K at $\epsilon = +7\%$, beyond which T_C turns to decrease. In contrast, the compressive strain can suppress T_C monotonously, e.g. to 0.295 K when biaxial strain down to $\epsilon = -5\%$.

Physically, a tensile strain suppresses the bilayer thickness and thus shortens the distance between Na and S1, which can result in more electron transfer from Na to S1 and improve the DOS at the Fermi level (as shown in Fig. 5(b)). In addition, tensile strain also leads to stronger electron-phonon interaction by softening the E'(TO), E'(LO), and A_2''(ZO) modes. Similar conclusion is also reached in $(MoSe_2)_2Na$ whose T_C is enhanced up to 3.944 K for $\epsilon = +5\%$ biaxial tensile strain but suppressed to near zero for compressive strain.

Previous studies suggested that in general the superconducting T_C of 2D materials could be improved by increasing doping density.[10,20,25] Our calculation gives one more route to improve T_C effectively and easily.

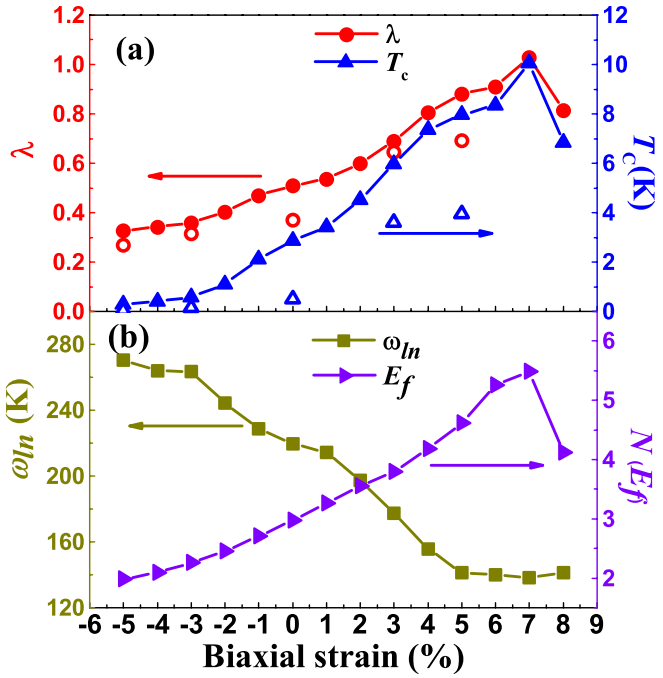

FIG. 5. (Color online) Calculated biaxial stress effects for $(MoX_2)_2Na$ (solid symbols: $(MoS_2)_2Na$; open symbols: $(MoSe_2)_2Na$). The dynamic stability for both cases persists within this strain region. (a) Superconducting T_C (right axis) and electron-phonon coupling λ (left axis). (b) Logarithmically averaged frequency ω_{ln} and electronic DOS at Fermi level $N(E_f)$.

C. Phonon mean free path

Finally, in order to deeply understand the lattice dynamics of Na-intercalated MoX_2, the phonon mean free path (MFP) is also investigated, which now can be directly measured in experiments.[26] The phonon MFP for the mode at q point with s polarization is defined as $Q_{qs} = V_{qs}\tau_{qs}$, where V_{qs} is the phonon group velocity and τ_{qs} is phonon relaxation time. In real materials, the phonon relaxation time is determined by the combination of electron-phonon, phonon-phonon umklapp scattering, and boundary scattering. For few-layer 2D materials, the boundary scattering from the sides should be very weak and negligible.[27] For simplify, a uniform lifetime (τ^{ep}) is assumed for all phonon modes' contributions to the electron-phonon scattering, and the Debye spectrum is adopted as the phonon density of state approximatively[28]. Then, $\alpha^2F(\omega)$ can be approximated as:[28]

$$\alpha^2F(\omega) \approx \frac{3(\tau^{ep})^{-1}}{2\pi N(E_f)}\frac{\omega}{\hbar\omega_{\rm D}^3}, \quad (4)$$

where $\omega_{\rm D}$ is the Debye frequency. Corresponding the λ can be integrated as:

$$\lambda = 2\int_0^\infty \frac{\alpha^2F(\omega)}{\omega}d\omega = \frac{6(\tau^{ep})^{-1}}{2\pi N(E_f)}\frac{1}{\hbar\omega_{\rm D}^2}. \quad (5)$$

TABLE IV. The calculated Debye frequency $\omega_{\rm D}$, phonon-phonon relaxation time (τ^{ph-ph}), electron-phonon relaxation time (τ^{ep}), and MPF for $(MoX_2)_2Na$ system around the Γ point at room temperature and at the frequency of 4 cm^{-1}.

	$\omega_{\rm D}$ (cm^{-1})	τ^{ph-ph} (ps)	τ^{ep} (ps)	MPF (nm)
$(MoS_2)_2Na$	237.0	237.4 (TA)	23.8	142.4 (TA)
		236.8 (LA)		229.9 (LA)
$(MoSe_2)_2Na$	171.9	1077.2 (TA)	68.5	536.2 (TA)
		913.6 (LA)		612.3 (LA)

Then using the value of λ calculated before, the effective τ^{ep} can be estimated, as presented in Table IV.

The three-phonon umklapp scattering lifetimes (τ^{ph-ph}) for different phonon branches can be estimated as:[29,30]

$$\tau_{qs}^{ph-ph} = (2\gamma_{qs}^2\frac{k_BT}{Mv_s^2}\frac{\omega_{qs}^2}{\omega_{\rm D}})^{-1}, \quad (6)$$

where M is the mass of a $(MoX_2)_2Na$ unit cell, v_s is the average phonon velocity for a given branch, T is temperature, k_B is the Boltzmann constant, and γ is the Grüneissen parameter. For 2D materials, the γ of each phonon mode at q point with s polarization is given by:[31,32]

$$\gamma_{qs} = -\frac{a}{2\omega_s(q)}\frac{d\omega_s(q)}{da} \quad (7)$$

Since the acoustic modes (particularly the LA and TA modes) have relatively larger velocities around the Γ point than those of the optical modes, they contribute to most of Q.[33] Here γ_{qs} is averaged around Γ point. The calculated MFP's of acoustic modes around the Γ point are listed in Table IV. The phonon-phonon umklapp scattering makes about 90% contributions to MFP for $(MoX_2)_2Na$. The anharmonic terms in lattice vibration have great influences on MFP and mainly reflect in γ here. Generally, larger γ leads to smaller MFP. For $(MoS_2)_2Na$, we obtain γ for TA and LA modes are 2.64 and 2.11 respectively, while in $(MoSe_2)_2Na$ are only 1.47 and 1.34 respectively. The stronger anharmonicity in $(MoS_2)_2Na$ leads to smaller MFP. Therefore, the MFP's (536.2 nm for the TA branch, 612.3 nm for the LA branch) in $(MoSe_2)_2Na$ is quite prominent, approaching that of graphene (about 775 nm).[34] Even for $(MoS_2)_2Na$, the MFP's (142.4 nm for the TA branch and 229.9 nm for the LA branch) are larger than those of monolayer MoS_2 (about 103.1 nm for the LA branch calculated using the same method). While in Ref. 35, the MFP for the LA branch was reported to be only 18.1 nm for MoS_2 monolayer, which was partially due to the inaccuracy γ in their calculation, as pointed out by Ref. 36 and 37. In short, the Na-intercalation can significantly improve the phonon mean free path of $(MoX_2)_2Na$, which may be used in heatconduction devices.

IV. CONCLUSION

An in-depth understanding of electronic properties, the lattice dynamical properties, and superconductivity of modificatory 2D materials is highly important for its potential applications in heatconduction devices as well as nanoscale superconductor. The present DFT study found that the Na atoms intercalation can effectively change the electronic properties and lattice dynamical properties of MoS_2 and $MoSe_2$.

In summary, electrons transfer from intercalated Na atoms to neighboring Se or S atoms, which increase the density of states at the Fermi level and a semiconducting-to-metallic transition. The superconductivity is expected to be induced by such Na-intercalation, and the superconducting T_C would be enhanced by biaxial tensile strain. In addition, the phonon mean free path at room-temperature is also greatly improved in Na intercalated $MoSe_2$, which is advantaged for related applications.

ACKNOWLEDGMENTS

Work was supported by National Natural Science Foundation of China (Grant Nos. 11274060 and 51322206).

* Corresponding author: sdong@seu.edu.cn

[1] B. Radisavljevic, A. Radenovic, J. Brivio, V. Giacometti, and A. Kis, Nature Nanotech. **6**, 147 (2011).
[2] Q. H. Wang, K. Kalantar-Zadeh, A. Kis, J. N. Coleman, and M. S. Strano, Nature Nanotech. **7**, 699 (2012).
[3] S. Sim, J. Park, J. G. Song, C. In, Y. S. Lee, H. Kim, and H. Choi, Phys. Rev. B **88**, 075434 (2013).
[4] H. Shi, R. Yan, S. Bertolazzi, J. Brivio, B. Gao, A. Kis, D. Jena, G. H. Xing, and L. Huang, ACS Nano **7**, 1072 (2013).
[5] K. Kaasbjerg, K. S. Thygesen, and K. W. Jacobsen, Phys. Rev. B **85**, 115317 (2012).
[6] K. Kaasbjerg, K. S. Thygesen, and A. P. Jauho, Phys. Rev. B **87**, 235312 (2013).
[7] J. L. Verble and T. J. Wieting, Phys. Rev. Lett. **25**, 362 (1970).
[8] K. Lee, W. S. Yun, and J. D. Lee, Phys. Rev. B **91**, 125420 (2015).
[9] Z. Y. Huang, G. L. Hao, C. Y. He, H. Yang, L. Xue, X. Qi, X. Y. Peng, and J. X. Zhong, J. Appl. Phys. **114**, 083706 (2013).
[10] Y. Z. Ge and A. Y. Liu, Phys. Rev. B **87**, 241408 (2013).
[11] J. A. Woollam and R. B. Somoano, Phys. Rev. B **13**, 3843 (1976).
[12] G. Q. Huang, Z. W. Xing, and D. Y. Xing, Phys. Rev. B **93**, 104511 (2016).
[13] P. Giannozzi, S. Baroni, N. Bonini, M. Calandra, R. Car, C. Cavazzoni, D. Ceresoli, G. L. Chiarotti, M. Cococcioni, and I. D. et al., J. Phys.: Condens. Matter **21**, 395502 (2009).
[14] S. Grimme, J. Comput. Chem. **27**, 1787 (2006).
[15] Q. H. Liu, L. Li, Y. F. Li, Z. X. Gao, Z. F. Chen, and J. Lu, J. Phys. Chem. C **116**, 21556 (2012).
[16] T. Böker, R. Severin, A. Müller, C. Janowitz, R. Manzke, D. Voss, P. Krüger, A. Mazur, and J. Pollmann, Phys. Rev. B **64**, 235305 (2001).
[17] L. M. Kulikov, A. A. S. Kobzar, L. G. Akselrud, T. A. Lobova, and E. A. Bogachev, Inorg. Mater. **28**, 397 (1992).
[18] T. Komesu, D. Le, X. Zhang, Q. Ma, E. F. Schwier, Y. Kojima, M. Zheng, H. Iwasawa, K. Shimada, M. Taniguchi, L. Bartels, T. S. Rahman, and P. A. Dowben, Appl. Phys. Lett. **105**, 241602 (2014).
[19] S.-Y. Chen, C. Zheng, M. S. Fuhrer, and J. Yan, Nano Lett. **15**, 2526 (2015).
[20] G. Q. Huang, Z. W. Xing, and D. Y. Xing, Appl. Phys. Lett. **106**, 113107 (2015).
[21] G. Grimvall, *The electron-phonon interaction in metals*, Vol. 8 (North-Holland Amsterdam, 1981).
[22] P. B. Allen and M. L. Cohen, Phys. Rev. **187**, 525 (1969).
[23] P. B. Allen and R. C. Dynes, Phys. Rev. B **12**, 905 (1975).
[24] F. Guinea, M. Katsnelson, and A. Geim, Nature Phys. **6**, 30 (2010).
[25] M. Q. Xue, G. F. Chen, H. X. Yang, Y. H. Zhu, D. M. Wang, J. B. He, and T. B. Cao, J. Am. Chem. Soc. **134**, 6536 (2012).
[26] A. J. Minnich, J. A. Johnson, A. J. Schmidt, K. Esfarjani, M. S. Dresselhaus, K. A. Nelson, and G. Chen, Phys. Rev. Lett. **107**, 095901 (2011).
[27] Z. Wang and N. Mingo, Appl. Phys. Lett. **99**, 101903 (2011).
[28] P. Souvatzis, J. Phys.: Condens. Matter **23**, 445401 (2011).
[29] P. G. Klemens, Journal of Wide Bandgap Materials **7**, 332 (2000).
[30] P. G. Klemens, Int. J. Thermophys. **22**, 265 (2001).
[31] J. Zou and A. Balandin, J. Appl. Phys. **89**, 2932 (2001).
[32] N. Mounet and N. Marzari, Phys. Rev. B **71**, 205214 (2005).
[33] Z. Y. Ong and E. Pop, Phys. Rev. B **84**, 075471 (2011).
[34] S. Ghosh, I. Calizo, D. Teweldebrhan, E. P. Pokatilov, D. L. Nika, A. A. Balandin, F. M. W. Bao, and C. N. Lau, Appl. Phys. Lett. **92**, 151911 (2008).
[35] Y. Q. Cai, J. H. Lan, G. Zhang, and Y. W. Zhang, Phys. Rev. B **89**, 035438 (2014).
[36] L. F. Huang, P. L. Gong, and Z. Zeng, Phys. Rev. B **90**, 045409 (2014).
[37] C. Sevik, Phys. Rev. B **89**, 035422 (2014).